Supplement of

Distinguishing subaerial and submarine calving with underwater noise

Oskar Glowacki

Institute of Geophysics, Polish Academy of Sciences

Correspondence to: oglowacki@igf.edu.pl

S1. Selection of input parameters in the semi-automatic algorithm for determining t_0 and t_1 of a calving event.

A visualization of the semi-automatic algorithm for determining the start and end times of a calving event is shown in Fig. S1. The algorithm requires six user-provided parameters:

(i) the nominal middle of a calving signal, t_{mid};

(ii) lower frequency limit, f_0;

(iii) upper frequency limit, f_1;

(iv) length of the median filter used to calculate the baseline power, Ψ;

(v) length of the median filter that eliminates short noise impulses not related to calving events, Γ;

(vi) maximum allowable separation between distinct noise signatures associated with a single calving event, τ_{max}.

The selection of the input parameters proceeds as follows.

First, the nominal middle of a calving signal is found by a visual inspection of a low pass filtered version of the recording (f_{cutoff} = 1 kHz) and a noise spectrogram (see Fig. S1A-D). The filter cutoff frequency of 1 kHz is based on previous studies that investigated the time and frequency structure of the calving noise (e.g., Glowacki, 2020; Glowacki and Deane, 2020). Calving signatures were always clearly distinguishable from the background noise. Importantly, the algorithm is not particularly sensitive to the selection of t_{mid}. Consequently, only the approximate value of t_{mid} is required.

Second, minimum and maximum allowable values of the remaining parameters are selected. The selection is based on the current understanding of the calving noise and the preliminary analysis of the data (e.g. computation of spectrograms). The lower frequency limit is assumed to be greater than 20 Hz to eliminate the possible contribution from the low-frequency flow noise (strum). The maximum value of the upper frequency limit is set to 1 kHz because higher-frequency noise in the glacial bay is generated mainly by submarine melting of glacier ice (e.g., Deane et al., 2014; Pettit et al., 2015; see also spectrograms in Fig. S1C-D). The length of the median filter applied to calculate the baseline power ranges between 30 and 120 s. The filter must be of a sufficient length to capture quiescent periods (calving-free noise segments). However, the value of Ψ should not be too high because the background noise level immediately after a subaerial calving event is usually strongly influenced by post-impact wave action (see spectrogram in Fig. S1C). Consequently, the median filter with a length higher than 120 s would make the algorithm for determining t_0 and t_1 very sensitive to surface wave conditions and the amount of ice on the sea surface (energetic interactions during mini-tsunamis). Noise impulses not related to calving events, including mechanical transients, are assumed to be shorter than 2.5 s; this assumption is based on the visual inspection of spectrograms and listening to the noise recordings. The separation between distinct noise signatures associated with individual calving events ranges from 5 to 20 s. The range of values for the parameter τ_{max} is estimated from noise recordings and high-frequency (1 Hz) GoPro images of calving events. Higher values of τ_{max} may result in treating two successive calving events as a single event. Conversely, lower values of τ_{max} may separate one event into several

events. For example, calving of highly-fragmented ice blocks often consists of several sub-events that form an ice avalanche.

Third, the final values of the input parameters are selected using the trial and error method. Data collected in 2016 (close buoy) are analyzed first. Plots similar to those shown in Fig. S1 are computed for every calving event; parameter values change in a loop within the allowed ranges (discussed in the preceding paragraph). The start and end times of the calving signal are plotted with vertical dashed lines that allow for evaluation of the algorithm performance (see Fig. S1E-F). The performance is evaluated for randomly selected events by comparison between the algorithm outputs and user expectations supported by visual inspection of spectrograms and listening to audio recordings. Importantly, the same values of input parameters must apply to subaerial and submarine events. Optimal values of input parameters are selected. Finally, the algorithm is tested using data collected in 2017 (far buoy) to check the algorithm performance in the case of a much lower signal-to-noise ratio. Changes to parameter values are made if necessary.

The following values of user-provided parameters were selected: $f_0 = 30$ Hz, $f_1 = 200$ Hz, $\Psi = 40$ s, $\Gamma = 2.3$ s, $\tau_{max} = 12$ s. This selection was a trade-off between the algorithm efficacy and its applicability to both subaerial and submarine events. For example, some other parameter values worked well for subaerial events but were not suitable for submarine events (and vice versa).

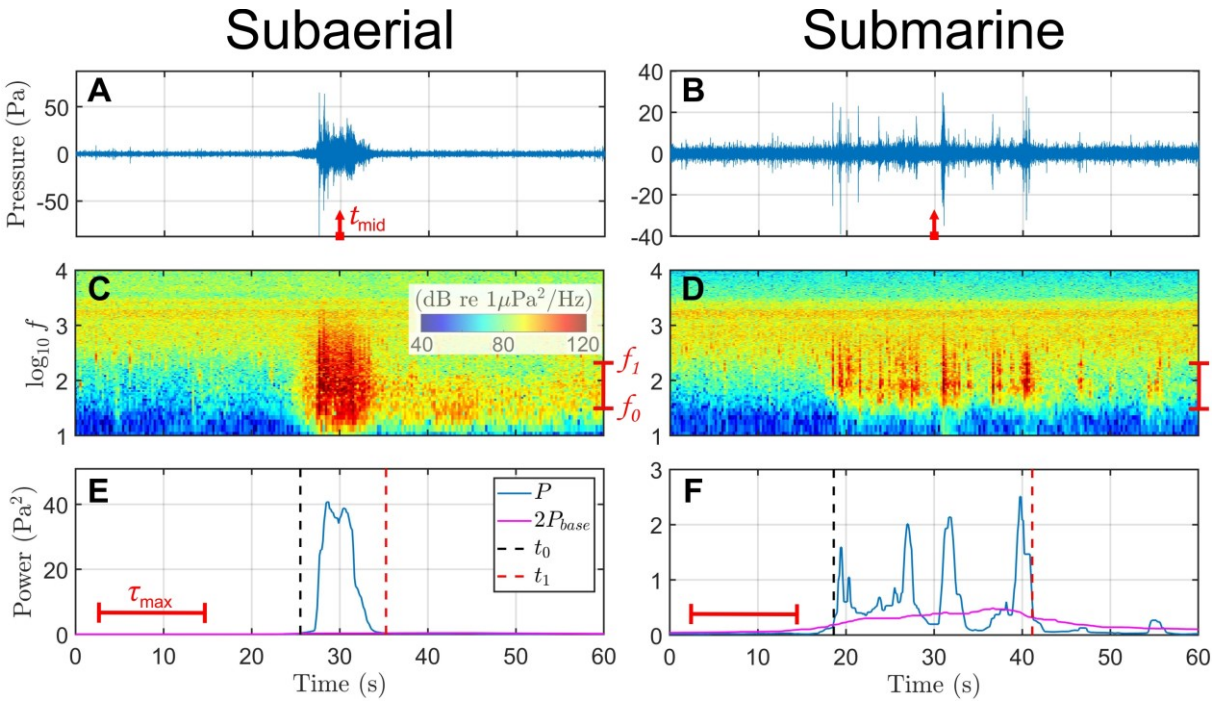

Figure S1. A visualization of the semi-automatic algorithm for determining start and end times of subaerial (**A,C,E**) and submarine (**B,D,F**) events. (**A-B**) Waveforms of the low-pass (< 1 kHz) filtered acoustic pressure. Each waveform is centered in the nominal middle of the calving signal. (**C-D**) Spectrograms of the acoustic recordings. Frequency limits used for the computation of the noise power are marked on the right edges of the spectrograms. (**E-F**) The median filtered ($\Gamma = 2.3$ s) noise power, baseline power multiplied by 2, and start and end times of calving events (as determined by the algorithm).

S2. Supplementary figure of the similarity between the calving noise parameters.

The figure below is analogous to Fig. 6 in the original manuscript but the calving noise parameters were computed for the 2017 data.

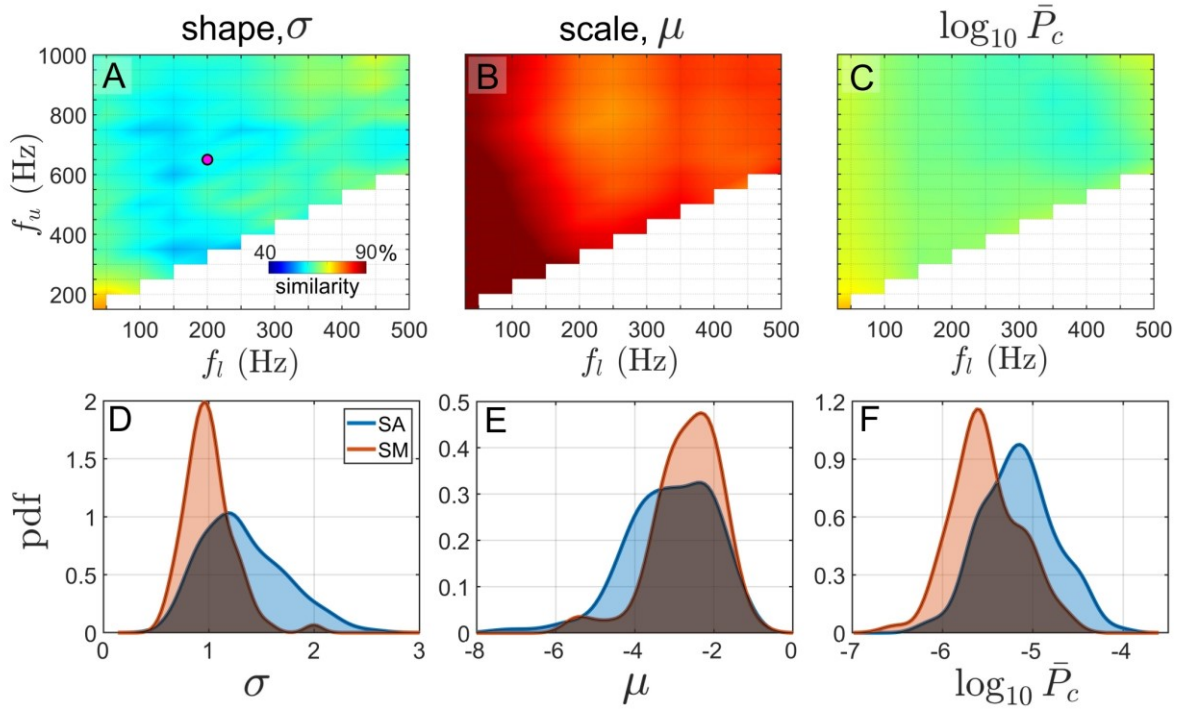

Figure S2. (**A-C**) Color plots of the similarity between probability density functions of parameters σ, μ and $\log_{10} \bar{P}_c$ calculated for SA and SM events observed in 2017. Variables f_l and f_u denote lower and upper integration limits, respectively. (**D-F**) Probability density functions estimated for the noise parameters using Matlab's kernel smoothing function (*ksdensity*; Hill, 1985); f_l = 200 Hz and f_u = 650 Hz (pink dot in panel **A**). Dark areas indicate overlaps between probability density functions used as a similarity measure in panels (**A-C**).

References

Deane GB, Glowacki O, Tegowski J, Moskalik M and Blondel P (2014) Directionality of the ambient noise field in an Arctic, glacial bay. The Journal of the Acoustical Society of America, 136(5), EL350–EL356 (doi: 471 10.1121/1.4897354)

Glowacki O (2020) Underwater noise from glacier calving: Field observations and pool experiment. The Journal of the Acoustical Society of America, 148(1), EL1–EL7 (doi: 10.1121/10.0001494)

Glowacki O and Deane GB (2020) Quantifying iceberg calving fluxes with underwater noise. The Cryosphere, 14(3), 1025–1042 (doi: 10.5194/tc-14-1025-2020)

Hill PD (1985) Kernel estimation of a distribution function. Communications in Statistics - Theory and Methods, 14(3), 605–620 (doi: 10.1080/03610928508828937)

Pettit EC, Lee KM, Brann JP, Nystuen JA, Wilson PS and O'Neel S (2015) Unusually loud ambient noise in tidewater glacier fjords: A signal of ice melt. Geophysical Research Letters, 42(7), 2309–2316 (doi: https://doi.org/10.1002/2014GL062950)